IEEE Access
Multidisciplinary | Rapid Review | Open Access Journal

Received March 27, 2018, accepted April 25, 2018, date of publication April 27, 2018, date of current version May 24, 2018.

Digital Object Identifier 10.1109/ACCESS.2018.2830967

Analysis and Design of M-Channel Hybrid Filter Bank With Digital Calibration

XIANGYU PENG[1], JINGYU LI[1], XIAOTIAN ZHOU[2], QIANQIANG LIN[1], AND ZENGPING CHEN[1]
[1]Science and Technology on Automatic Target Recognition Laboratory, National University of Defense Technology, Changsha 410073, China
[2]Target Support Brigade of STCJOCC, Guangzhou 510000, China

Corresponding author: Xiangyu Peng (xiangyu_peng@163.com)

ABSTRACT Hybrid filter bank (HFB) is widely used in frequency-interleaved analog-to-digital converters, but traditional HFB structures suffer various degrees of imperfections. This paper presents a new-structure HFB based on power complementary pair. The proposed architecture only needs M-1 analog analysis filters in M-channel frequency-interleaved analog-to-digital converters, and the analog analysis filters can satisfy the pairwise power complementary property. Therefore, the new structure simplifies analog circuits to a larger extent compared with traditional structure. Based on the proposed structure, an estimation algorithm is put forward to estimate the channel mismatch errors and filter bank mismatch errors. Accordingly, calibration is carried out in digital domain. Experiments are performed on the basis of designing a four-channel 20 GS/s 12-bit frequency-interleaved analog-to-digital converter system, and the simulation results prove the effectiveness of the proposed method. Average distortion error of -6.8192×10^{-10} dB and an average aliasing error of -104.84dB can be achieved after calibration, and resolution of this architecture can be up to 14 bit.

INDEX TERMS Channel mismatch errors, filter bank mismatch errors, frequency-interleaved analog-to-digital converter, hybrid filter bank, power complementary pair.

I. INTRODUCTION

Signal sampling system of modem information equipment such as radar, holds an ever-increasing high requirement for both the resolution and the sampling rate of analog-to-digital converters (ADCs). However, single ADC can satisfy neither of them at the same time.

Multi-channel structure plays a pivotal role in many implementations to design High-speed and High-resolution ADC system [1]–[3]. Theoretically, multiple-channel structure improves the sampling rate proportionally with the increasing number of channels. Nevertheless, the mismatch between channels makes the performance worse than expected in practice.

Time-interleaved ADC (TIADC) is firstly studied, which is extremely sensitive to time skew. Since the time skew problem of TIADC is strongly correlative with the frequency of input signals [4]. There are many publications [5]–[7] which have presented several calibration methods. However, it is not suitable for a high resolution especially in the high bandwidth (up to GHz) implementation [8]. The parallel ADC structure based on quadrature mirror filter bank (QMFB) overcomes the disadvantage of TIADC [9], but switch-capacitor filters limit the speed of the system and introduce switching noise, which may degrade the performance of designed system.

Hybrid filter bank (HFB) is similar to QMFB in principle. Fig. 1(a) shows the prototype HFB, where Ω is defined as the analog angular frequency and $\omega = \Omega T_s$ is the digital angular frequency. The analog analysis filter bank divides the overall input signal frequency band symmetrically, as shown in Fig. 1(b) where Ω_c is the cut-off frequency of input signal. The allocated sub-bands are sampled by ADCs in different channels, and the sampled data is reconstructed via digital synthesis filters after up-sampling at [10] and [11]. However, constructing a traditional structure of HFB faces many challenges. The mixed channel mismatch error and filter bank mismatch error make the estimation and calibration difficult. In literature [12], a calibration method of filter bank mismatches was proposed which, however, fails in considering the channel mismatches. In literature [13], the effect of the channel mismatches on the Frequency-Interleaved analog-to-digital converter (FIADC) system has been analyzed, yet, it did not set forth a calibration method. There was a blind estimation method for the analog filter parameters in [14], but this method needs oversampling and can only be used to

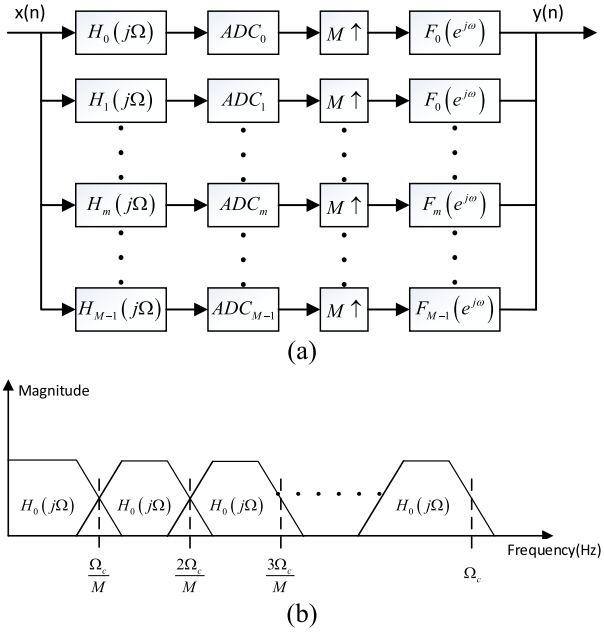

FIGURE 1. **(a) *M*-channel FIADC structure. (b) The frequency distribution of *M*-channel analysis filter bank.**

calibrate filter bank mismatch error. Therefore, it is necessary to propose a joint calibration method that can calibrate two kinds of errors synchronously.

Another challenge lies in how to design analog and digital filters to ensure adequate channel separation and accurate reconstruction of the converted signal. In the traditional structure of HFB, the analog analysis filters shall be designed as low-pass, band-pass and high-pass and divide the input signal into several sub-band signals symmetrically [15], [16]. To minimize the filter bank mismatch error (i.e., distortion error caused by the unsatisfactory amplitude-frequency characteristic of analog analysis filters and aliasing error caused by the mirroring due to the sampling and interpolation), filters need to be properly designed so as to present good filter characteristics like sharp cutoff and large stopband attenuation which will increase the order of analog analysis filter.

Literature [17] presents mixed norm optimal design of digital synthesis filter to compensate the inadequacies of analog analysis filter. Literature [18] proposed a cosine modulated HFB. However, they all base on traditional HFB structure. A power complementary pair-based structure of HFB is proposed in [19]. Regardless of sharp cutoff and large stopband attenuation, the analog filters of this structure only need to show a power complementary. However, it can only be used in the two-channel FIADC. This paper proposes a tree-structure of HFB based on power complementary pairs. The analog analysis filters aim to decompose the input signal to alleviate the requirement of the ADCs rather than channeling frequency domain into sub-bands. The filter of this HFB does not need narrow transition width which is inversely proportional to the order of the filter, therefore, high filter order can be avoided. To minimize the distortion error and aliasing error, a corresponding calibration technique is presented which can calibrate filter bank mismatch error and channel mismatch error such as offset as well as gain mismatch error in the meantime.

II. TREE-STRUCTURE HFB BASED ON POWER COMPLEMENTARY PAIRS

The output of M-channel HFB shown in Fig. 1 (a) can be expressed as [10]

$$Y\left(e^{j\omega}\right)=\frac{1}{MT_s}\sum_{p=0}^{M-1}X\left(j\frac{\omega}{T_s}-j\frac{2\pi p}{MT_s}\right)T_p\left(e^{j\omega}\right), \quad (1)$$

where MT_S is a sampling period of single ADC. The system transfer function is given as,

$$T_p\left(e^{j\omega}\right)=\frac{1}{MT_s}\sum_{m=0}^{M-1}H_m\left(j\frac{\omega}{T_S}-j\frac{2\pi p}{MT_S}\right)F_m\left(e^{j\omega}\right), \quad (2)$$

where m is the serial number of sub-channel, H_m is the analog analysis filter transfer function of the m^{th} channel, and F_m is transfer function of the m^{th} digital synthesis filter. For perfect reconstruction, the ideal distortion function $T_0\left(e^{j\omega}\right)$ should be the delayed and scaled version of input signal, while the ideal aliasing function $T_p\left(e^{j\omega}\right), 1<p\leq M-1$ should be zero. Therefore, the perfect reconstruction (PR) condition [20] of the M-channel FIADC is expressed as,

$$\begin{cases}\dfrac{1}{MT_s}\displaystyle\sum_{m=0}^{M-1}H_m\left(j\frac{\omega}{T_S}\right)F_m\left(e^{j\omega}\right)=ce^{-j\omega d}\\ \dfrac{1}{MT_s}\displaystyle\sum_{m=0}^{M-1}H_m\left(j\frac{\omega}{T_S}-j\frac{2\pi p}{MT_S}\right)F_m\left(e^{j\omega}\right)=0,\end{cases} \quad (3)$$

where c is nonzero constant referred to as the scale factor and d is the system delay. In accordance with the principle of the two-channel HFB in [19], Fig. 2 displays a power complementary pairs-based M-channel tree-structure HFB, where $M=2^N$.

The analog power complementary filter pair V_0 and W_0 decomposes the ideal time-frequency plane. Then another analog power complementary filter pair V_1 and W_1 decomposes the output signal of V_0 and so on. After N times of decomposition, N pairs of analog analysis filters decompose the input signal into M analog signals. Each signal is sampled by ADCs whose sampling rate is one in M sampling rate of system. Then M digital signals can be obtained. Each digital signal is up-sampled by M and filtered by digital synthesis filter pair C_{N-1} and D_{N-1} respectively. $M/2$ digital signals can be obtained after filtered signals paired addition. The above operation shall be repeated until all signals are merged into one, then perfect reconstruction digital signal can be achieved. When N equals to one, the tree-structure HFB becomes two-channel HFB based on power complementary pair described in [19].

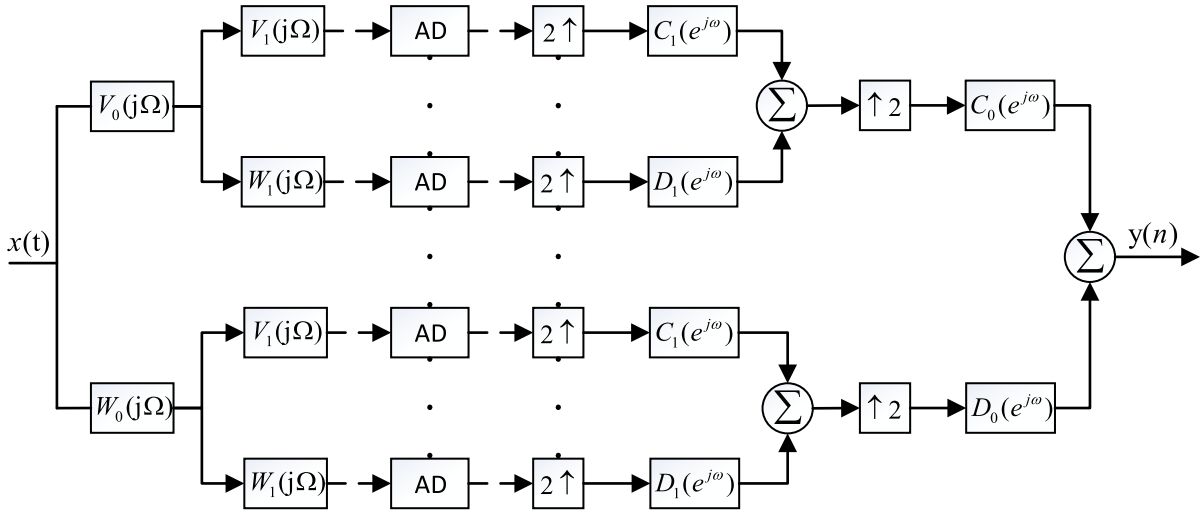

FIGURE 2. *M*-channel tree-structure hybrid filter bank.

Each channel has N analog filters and N digital filters. The equivalent analog filter function $H_m(j\Omega)$ and digital filter transfer function $F_m(e^{j\omega})$ of each channel are expressed as,

$$H_m(j\Omega) = \prod_{k=0}^{N-1} S(j\Omega, m, k)$$
$$S(j\Omega, m, k) = \begin{cases} V_k(j\Omega), & \lfloor i/2^{N-k-1} \rfloor - 2\lfloor i/2^{N-1} \rfloor = 0 \\ W_k(j\Omega), & \lfloor i/2^{N-k-1} \rfloor - 2\lfloor i/2^{N-1} \rfloor = 1 \end{cases} \tag{4}$$

and

$$F_m\left(e^{j\omega}\right) = \prod_{k=0}^{N-1} R(j\omega, m, k)$$
$$R(j\omega, m, k) = \begin{cases} C_k\left(e^{j\omega 2^k}\right), & \lfloor i/2^{N-k-1} \rfloor \\ \quad -2\lfloor i/2^{N-1} \rfloor = 0 & \\ D_k\left(e^{j\omega 2^k}\right), & \lfloor i/2^{N-k-1} \rfloor \\ \quad -2\lfloor i/2^{N-1} \rfloor = 1, & \end{cases} \tag{5}$$

where $\lfloor X \rfloor$ is the rounding off of X, $k = 0, 1, 2 \ldots N-1$ is serial number of filters and $m = 0, 1, 2 \ldots M-1$ is serial number of channels.

From (3), (4), and (5), the PR condition of the M-channel tree-structure FIADC can be expressed as (assume $MT_s = \frac{1}{c}$),

$$\begin{cases} \prod_{k=0}^{N-1} \left[V_k\left(j\frac{\omega}{T_s}\right) C_k\left(e^{j\omega 2^k}\right) + W_k(j\frac{\omega}{T_s}) D_k\left(e^{j\omega 2^k}\right) \right] \\ \quad = e^{-j\omega d} \\ \prod_{k=0}^{N-1} \left[V_k\left(j\frac{\omega}{T_s} - j\frac{2\pi p}{MT_s}\right) C_k\left(e^{j\omega 2^k}\right) \right. \\ \quad \left. + W_k\left(j\frac{\omega}{T_s} - j\frac{2\pi p}{MT_s}\right) D_k\left(e^{j\omega 2^k}\right) \right] = 0. \end{cases} \tag{6}$$

III. DESIGN OF HYBRID FILTER BANK

It is not necessary to design the analog analysis filters of tree-structure HFB as low-pass, band-pass and high-pass. They only need to satisfy perfect reconstruction condition in (6). Based on the Mathematical Deduction, we can prove the lemma: the analog analysis filters can meet the PR condition expressed in (6) in premise of satisfying the following condition

$$\begin{cases} V_k\left(j\frac{\omega}{T_s}\right) C_k\left(e^{j\omega 2^k}\right) + W_k\left(j\frac{\omega}{T_s}\right) D_k\left(e^{j\omega 2^k}\right) = e^{-j\omega d_k} \\ V_k\left(j\frac{\omega}{T_s} - j\frac{\pi q}{2^k T_s}\right) C_k\left(e^{j\omega 2^k}\right) \\ \quad + W_k\left(j\frac{\omega}{T_s} - j\frac{\pi q}{2^k T_s}\right) D_k\left(e^{j\omega 2^k}\right) = 0, \end{cases} \tag{7}$$

where q is an odd number and is no more than 2^k, and the system delay satisfies

$$d = \sum_{k=0}^{N-1} d_k. \tag{8}$$

Proof: For $N = 1$, we can see that equation (6) is same as equation (7). So the lemma is true when $N = 1$.

Assume that the lemma is true when $N = r$, where r is a positive integer. Therefore, when p is an odd number which is no more than 2^r and $0 \le k \le r-1$,

$$\begin{cases} V_k\left(j\frac{\omega}{T_s}\right) C_k\left(e^{j\omega 2^k}\right) + W_k\left(j\frac{\omega}{T_s}\right) D_k\left(e^{j\omega 2^k}\right) = e^{-j\omega d_k} \\ V_k\left(j\frac{\omega}{T_s} - j\frac{\pi p}{2^k T_s}\right) C_k\left(e^{j\omega 2^k}\right) \\ \quad + W_k\left(j\frac{\omega}{T_s} - j\frac{\pi p}{2^k T_s}\right) D_k\left(e^{j\omega 2^k}\right) = 0. \end{cases} \tag{9}$$

For $N = r+1$. Let $d_r = d - \sum_{k=0}^{r-1} d_k$, from (6) and (9), we can get,

$$V_r\left(j\frac{\omega}{T_s}\right) C_r\left(e^{j\omega 2^r}\right) + W_r\left(j\frac{\omega}{T_s}\right) D_r\left(e^{j\omega 2^r}\right) = e^{-j\omega d_r}. \tag{10}$$

When p is an even number and no more than 2^{r+1}, we can deduce that at least one multiplication factor in (6) equals to zero according (9). Therefore, (6) is tenable in this case.

When p is an odd number and no more than 2^{r+1}. From (7), we can get,

$$V_r\left(j\frac{\omega}{T_s}-j\frac{2\pi q}{MT_s}\right)C_r\left(e^{j\omega 2^r}\right) + W_r\left(j\frac{\omega}{T_s}-j\frac{2\pi q}{MT_s}\right)D_r\left(e^{j\omega 2^r}\right)=0 \quad (11)$$

where $M=2^N=2^{r+1}$. Accordingly, (6) is tenable. In summary, we can conclude that the lemma is true. Equation (7) can serve as the PR condition.

In the case that the digital synthesis filters can be designed as delayed conjugations of the two analog analysis filters, that is $C_k\left(e^{j\omega 2^k}\right)=V_k\left(-j\frac{\omega}{T_S}\right)e^{-j\omega d_k}$ and $D_k\left(e^{j\omega 2^k}\right)=W_k\left(-j\frac{\omega}{T_S}\right)e^{-j\omega d_k}$ while $-\pi<\omega<\pi$, based on (7), the power complementary condition can be shown as,

$$\begin{aligned}&V_k\left(j\frac{\omega}{T_s}\right)V_k\left(-j\frac{\omega}{T_s}\right)\\&\quad+W_k\left(j\frac{\omega}{T_s}\right)W_k\left(-j\frac{\omega}{T_s}\right)=1\\&V_k\left(j\frac{\omega}{T_s}-j\frac{\pi p}{2^kT_s}\right)V_k\left(-j\frac{\omega}{T_s}\right)\\&\quad+W_k\left(j\frac{\omega}{T_s}-j\frac{\pi p}{2^kT_s}\right)W_k\left(-j\frac{\omega}{T_s}\right)=0\end{aligned} \quad (12)$$

Respectively define analog filter transfer functions $V_k(j\Omega)$ and $W_k(j\Omega)$ as,

$$V_k(j\Omega)=\frac{E_k(j\Omega)}{E_k(j\Omega)+O_k(j\Omega)} \quad (13)$$

and

$$W_k(j\Omega)=\frac{O_k(j\Omega)}{E_k(j\Omega)+O_k(j\Omega)}, \quad (14)$$

where $E_k(j\Omega)=\sum_n a_n(j\Omega)^n(n=even\ \text{number}\ \&\ n\le N_k-1)$ is the even part of the polynomial $B_k(j\Omega)$, and $O_k(j\Omega)=\sum_n a_n(j\Omega)^n(n=odd\ \text{number}\ \&\ n\le N_k-1)$ is the odd part of the polynomial $B_k(j\Omega)$ which is defined as,

$$B_k(j\Omega)=\sum_{n=0}^{N_k}a_n(j\Omega)^n, \quad (15)$$

N_k is the order of the filter and a_n is the n$^{\text{th}}$ polynomial of the denominator.

According to (13) and (14), it is easy to observe that

$$\begin{cases}V_k\left(j\frac{\omega}{T_s}\right)V_k\left(-j\frac{\omega}{T_s}\right)+W_k\left(j\frac{\omega}{T_s}\right)W_k\left(-j\frac{\omega}{T_s}\right)=1\\W_k\left(j\frac{\omega}{T_s}\right)V_k\left(-j\frac{\omega}{T_s}\right)+V_k\left(j\frac{\omega}{T_s}\right)W_k\left(-j\frac{\omega}{T_s}\right)=0.\end{cases} \quad (16)$$

To satisfy (12), use Genetic algorithm [21] to design the analog filters with the objective function defined as,

$$\Phi=\int_0^\pi\sum_q\left|V_k\left(j\frac{\omega}{T_s}\right)-W_k\left(j\frac{\omega}{T_s}-j\frac{\pi q}{2^kT_s}\right)\right|d\omega \quad (17)$$

where q is an odd number which is less than or equal to 2^k.

From equation (3), we can get,

$$\mathbf{H}(j\omega)\,\mathbf{F}\left(e^{j\omega}\right)=\mathbf{E}\left(e^{j\omega}\right), \quad (18)$$

where $\mathbf{F}\left(e^{j\omega}\right)=\left[F_0\left(e^{j\omega}\right)\cdots F_M\left(e^{j\omega}\right)\right]^T$ is the vector of frequency response for synthesis filters expressed in (5), and $\mathbf{H}(j\omega)$ is the matrix of analog filters' transfer function which is expressed in (4) and (19), as shown at the bottom of the next page, and $\mathbf{E}\left(e^{j\omega}\right)$ is the vector of frequency response for the distortion and aliasing transfer functions

$$\mathbf{E}\left(e^{j\omega}\right)=\left[e^{j\omega d}\quad 0\quad\cdots\quad 0\right]^T. \quad (20)$$

Using the inversion of matrix $\mathbf{H}(j\omega)$ to solve the (18), we can get the expression of digital filters.

$$\mathbf{F}\left(e^{j\omega}\right)=\mathbf{H}(j\omega)^{-1}\,\mathbf{E}\left(e^{j\omega}\right). \quad (21)$$

Then design digital synthesis filters using inverse fast Fourier transform: given the system delay d and N sample of the synthesis filter Fourier transform $F_m\left(e^{j\omega}\right)\big|_{\omega=(2\pi p/N)}$ $(p=0,1\ldots N-1)$. N should be large enough thus the impulse response has been sufficiently decayed so that the time aliasing will be negligible (e.g., $N=2048$), therefore, the definition of the N-point inverse fast Fourier transform is expressed as,

$$f_m^{(N)}(n)\approx\frac{1}{2\pi}\int_{-\pi}^{\pi}F_m\left(e^{j\omega}\right)e^{j\omega n}d\omega. \quad (22)$$

However, given that the resulting N-point impulse response is too long, we windowed it with rectangle window function (length L)

$$\hat{f}_m[n]=f_m^{(N)}[n]\,\omega[n], \quad (23)$$

where the rectangle window function is

$$\omega[n]=\begin{cases}1, & 0\le n\le L-1\\0, & L\le n\le N.\end{cases} \quad (24)$$

Then we adjusted the system delay d and the window length L, until the joint error function is minimized.

$$\varepsilon=\sum_{m=0}^{M-1}\sum_{n=L}^{N}\left(f_m^{(N)}[n]\right)^2. \quad (25)$$

To simplify the operation of digital synthesis filters, tree structure is not adopted in digital synthesis filter bank. Therefore, we can simplify the digital part of Fig. 2. The simplified tree-structure HFB is shown in Fig. 3. We finally designed four 64-lengh FIR digital filters and the system delay $d=32$ with the joint error less than 2.04×10^{-12}.

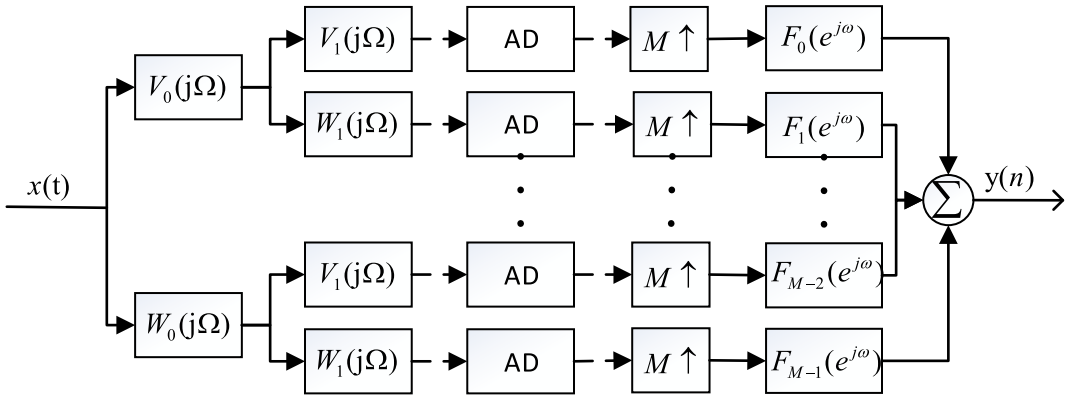

FIGURE 3. Simplified *M*-channel tree-structure hybrid filter bank.

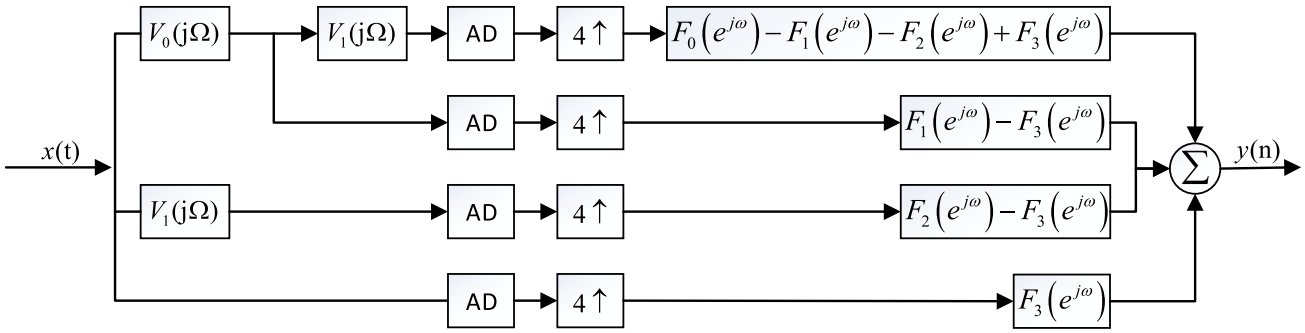

FIGURE 4. A improved tree-structure of four-channel hybrid filter bank.

IV. IMPROVED STRUCTURE OF FOUR-CHANNEL HFB

The analog filter pair V_k, W_k and the corresponding digital filter pair C_k, D_k constitute a two-channel HFB. Therefore, the tree structure greatly improves the complexity of analog circuit and digital operation. There are $M-1$ two-channel filter banks in M-channel tree-structure HFB. The number of analog analysis filters in tree-structure HFB is far beyond that in HFB with traditional structure. Moreover, we will propose an improved structure. From transfer function of analog analysis filters, shown in (13) and (14), it is easy to observe that

$$W_k(j\Omega) = 1 - V_k(j\Omega). \tag{26}$$

For the four-channel structure, we can get

$$\begin{cases} H_0(j\Omega) = V_0(j\Omega)\, V_1(j\Omega) \\ H_1(j\Omega) = V_0(j\Omega) - V_0(j\Omega)\, V_1(j\Omega) \\ H_2(j\Omega) = V_1(j\Omega) - V_0(j\Omega)\, V_1(j\Omega) \\ H_3(j\Omega) = 1 - V_0(j\Omega) - V_1(j\Omega) + V_0(j\Omega)\, V_1(j\Omega). \end{cases} \tag{27}$$

The system transfer function described in (2) can be rewritten as

$$\begin{aligned} T_p\left(e^{j\omega}\right) = {} & V_0(j\omega_p)V_1(j\omega_p) \\ & \times \left[F_0\left(e^{j\omega}\right) - F_1\left(e^{j\omega}\right) - F_2\left(e^{j\omega}\right) + F_3\left(e^{j\omega}\right)\right] \\ & + V_0\left(j\omega_p\right)\left[F_1\left(e^{j\omega}\right) - F_3\left(e^{j\omega}\right)\right] + F_3\left(e^{j\omega}\right) \\ & + V_1\left(j\omega_p\right)\left[F_2\left(e^{j\omega}\right) - F_3\left(e^{j\omega}\right)\right], \end{aligned} \tag{28}$$

where $\omega_p = \frac{\omega}{T_s} - \frac{2\pi p}{MT_s}$. Accordingly, the four-channel tree structure of HFB can be simplified, as shown in Fig. 4. This four-channel tree structure of HFB structure only needs three analog analysis filters. The method can be used in the other tree-structure HFB which has 2^N channels and only needs $2^N - 1$ analog analysis filters. It can reduce the error caused by the difference among the analog analysis filters.

V. CHANNEL MISMATCH ERROR AND FILTER MISMATCH ERROR CALIBRATION

Considering that the channel mismatch error and filter banks mismatch error have a substantial overlap, it is difficult to estimate and calibrate separately. To overcome this difficulty,

$$\begin{bmatrix} H_0(j\omega) & \cdots & H_{M-1}(j\omega) \\ \vdots & H_m\left(j\omega - j\frac{2\pi p}{M}\right) & \vdots \\ H_0\left(j\omega - j\frac{2\pi(M-1)}{M}\right) & \cdots & H_{M-1}\left(j\omega - j\frac{2\pi(M-1)}{M}\right) \end{bmatrix} \tag{19}$$

$$\begin{aligned}
\hat{V}_0(j\Omega) &= \frac{a_0'(j\Omega)^2 + a_2'}{(j\Omega)^3 + a_0'(j\Omega)^2 + a_1'(j\Omega) + a_2'} \\
\hat{V}_{10}(j\Omega) &= \frac{a_3'(j\Omega)^4 + a_5'(j\Omega)^2 + a_7'}{(j\Omega)^5 + a_3'(j\Omega)^4 + a_4'(j\Omega)^3 + a_5'(j\Omega)^2 + a_6'(j\Omega) + a_7'} \\
\hat{V}_{12}(j\Omega) &= \frac{b_3'(j\Omega)^4 + b_5'(j\Omega)^2 + b_7'}{(j\Omega)^5 + b_3'(j\Omega)^4 + b_4'(j\Omega)^3 + b_5'(j\Omega)^2 + b_6'(j\Omega) + b_7'},
\end{aligned} \tag{29}$$

we propose a combined correction algorithm. Taking the four-channel HFB as an example, $V_0(j\Omega)$ is the third-order analog filter and $V_1(j\Omega)$ is the fifth-order analog filter. The error model of system mismatch is shown in Fig. 5. Δg_m is gain ratio between the m^{th} channel and the 3^{th} channel, o_m is offset mismatch of each channel, $\hat{V}_{10}(j\Omega)$ and $\hat{V}_{12}(j\Omega)$ are corresponding to different deviations of $V_1(j\Omega)$, $\hat{F}_m(e^{j\omega})$ is equivalent digital filter. A method has been in Section III to calculate the parameter of analog filters. However, inevitably there are various practical errors such as parasitic resistance and parasitic capacitance. Which could lead to the deviation of $V_k(j\Omega)$. On that account, analog filter transfer functions of Fig. 5 with bias are expressed as in (29), as shown at the top of this page, where $a_n' = (1+\varepsilon_n)a_n$, ε_n is analog deviation factor of a_n. Similarly, $b_n' = (1+\partial_n)a_n$. Digital filter transfer functions in Fig. 5 are given by:

$$\begin{aligned}
\hat{F}_0(e^{j\omega}) &= \frac{1}{1+\Delta g_0}\left[F_0\left(e^{j\omega}\right) - F_1\left(e^{j\omega}\right) - F_2\left(e^{j\omega}\right) + F_3\left(e^{j\omega}\right)\right] \\
\hat{F}_1(e^{j\omega}) &= \frac{1}{1+\Delta g_1}\left[F_1\left(e^{j\omega}\right) - F_3\left(e^{j\omega}\right)\right] \\
\hat{F}_2(e^{j\omega}) &= \frac{1}{1+\Delta g_2}\left[F_2\left(e^{j\omega}\right) - F_3\left(e^{j\omega}\right)\right] \\
\hat{F}_3(e^{j\omega}) &= F_3\left(e^{j\omega}\right),
\end{aligned} \tag{30}$$

Define the outputs of ADCs as $X_m(j\Omega)$ expressed as,

$$\begin{cases}
X_0(j\Omega) = \frac{1}{4T}\left[\sum_{q=-\infty}^{\infty} X\left(j\Omega - j\frac{\pi q}{2T_s}\right)\hat{H}_0\left(j\Omega - j\frac{\pi q}{2T_s}\right) + 2\pi o_0\delta\left(j\Omega - j\frac{\pi q}{2T_s}\right)\right] \\
X_1(j\Omega) = \frac{1}{4T}\left[\sum_{q=-\infty}^{\infty} X\left(j\Omega - j\frac{\pi q}{2T_s}\right)\hat{H}_1\left(j\Omega - j\frac{\pi q}{2T_s}\right) + 2\pi o_1\delta\left(j\Omega - j\frac{\pi q}{2T_s}\right)\right] \\
X_2(j\Omega) = \frac{1}{4T}\left[\sum_{q=-\infty}^{\infty} X\left(j\Omega - j\frac{\pi q}{2T_s}\right)\hat{H}_2\left(j\Omega - j\frac{\pi q}{2T_s}\right) + 2\pi o_2\delta\left(j\Omega - j\frac{\pi q}{2T_s}\right)\right] \\
X_3(j\Omega) = \frac{1}{4T}\left[\sum_{q=-\infty}^{\infty} X\left(j\Omega - j\frac{\pi q}{2T_s}\right) + 2\pi o_3\delta\left(j\Omega - j\frac{\pi q}{2T_s}\right)\right],
\end{cases} \tag{31}$$

where $\hat{H}_m(j\Omega)$ is analog part transfer function of the m^{th} channel.

$$\begin{cases}
\hat{H}_0(j\Omega) = \hat{V}_0(j\Omega)\hat{V}_{10}(j\Omega)(1+\Delta g_0) \\
\hat{H}_1(j\Omega) = \hat{V}_0(j\Omega)(1+\Delta g_1) \\
\hat{H}_2(j\Omega) = \hat{V}_{12}(j\Omega)(1+\Delta g_2).
\end{cases} \tag{32}$$

Set the input signal $x(t) = \sin(\Omega_o t)$, the frequency of input signal should be smaller than the sampling frequency of single ADC. Define $x_m(n)$ $(m = 0, 1, 2)$ as the time domain expression of $X_m(j\Omega)$. From (31),

$$x_m(n) = G_m \sin(4nT_s\Omega_o) + o_m \ (m = 0, 1, 2, 3), \tag{33}$$

where G_m is the gain of the m^{th} channel. After taking out N points sampling data and adding them together, we can calculate offset error,

$$o_m = \lim_{N\to\infty}\frac{1}{N}\sum_{n=0}^{N-1}[G_m \sin(4nT_s\Omega_c) + o_m]. \tag{34}$$

The larger the N is, the more accurate the result of (34) will be. After the offset error is subtracted from the sampling results, the offset mismatches can be calibrated.

Next, we calibrate the gain errors and analog filter deviation. Assuming that the offset mismatch error has been calibrated. From (31), following equitation can be obtained according to Parseval's Theorem,

$$\begin{aligned}
\left|\hat{H}_0(j\Omega)\right|^2 &= \sum_{n=0}^{N-1}|x_0(n) - o_0|^2 \Big/ \sum_{n=0}^{N-1}|x_3(n) - o_3|^2 \\
\left|\hat{H}_1(j\Omega)\right|^2 &= \sum_{n=0}^{N-1}|x_1(n) - o_1|^2 \Big/ \sum_{n=0}^{N-1}|x_3(n) - o_3|^2. \\
\left|\hat{H}_2(j\Omega)\right|^2 &= \sum_{n=0}^{N-1}|x_2(n) - o_2|^2 \Big/ \sum_{n=0}^{N-1}|x_3(n) - o_3|^2
\end{aligned} \tag{35}$$

From (29) and (32), we can find that $\hat{H}_1(j\Omega)$ has four unknowns (ε_0, ε_1, ε_2 and Δg_1), $\hat{H}_2(j\Omega)$ has six unknowns (∂_3, ∂_4, ∂_5, ∂_6, ∂_7 and Δg_2), and $\hat{H}_0(j\Omega)$ has nine unknowns (ε_0, ε_1, ε_2, ε_3, ε_4, ε_5, ε_6, ε_7 and Δg_0), however, value of ε_0, ε_1 and ε_2 can be obtained by calculating $\hat{H}_1(j\Omega)$. Therefore, we can get the analog filter deviation factors ε_n, ∂_n and gain ratios Δg_m by Importing six various calibration cosine signals which frequencies are different and are all smaller than sampling frequency of single ADC. Substituting (32) into (21), the estimation of $F_m\left(e^{j\omega}\right)$ can be got. Finally, we use the digital filters to calibrate errors.

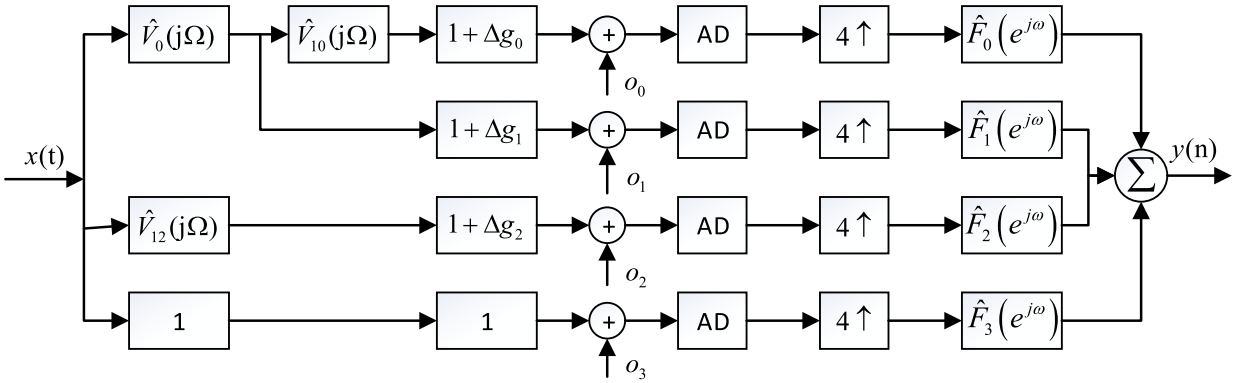

FIGURE 5. Error model of filter bank mismatches and channel mismatch.

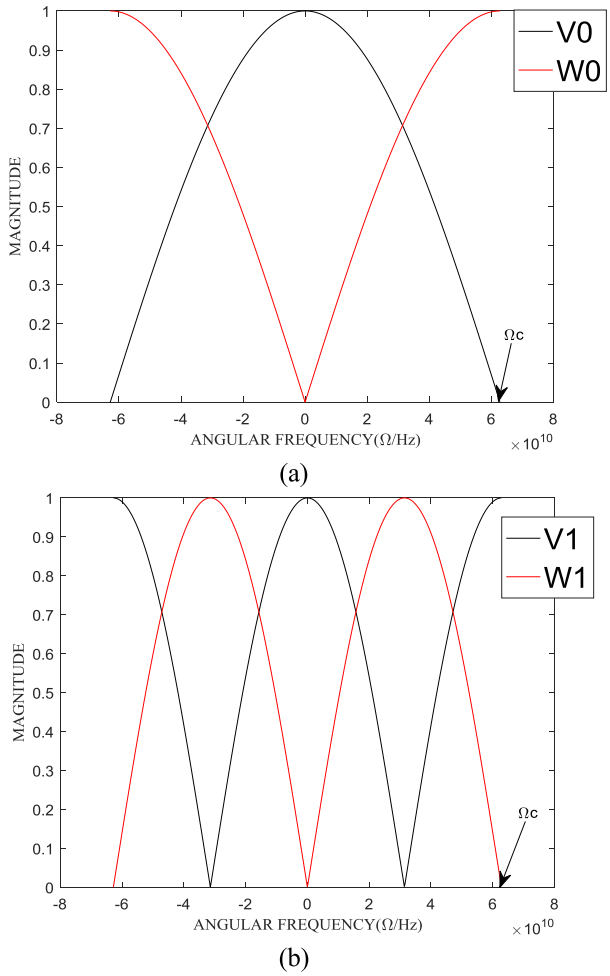

FIGURE 6. (a) The amplitude-frequency curve of third-order analog filters. (b) The amplitude-frequency curve of fifth-order analog filters.

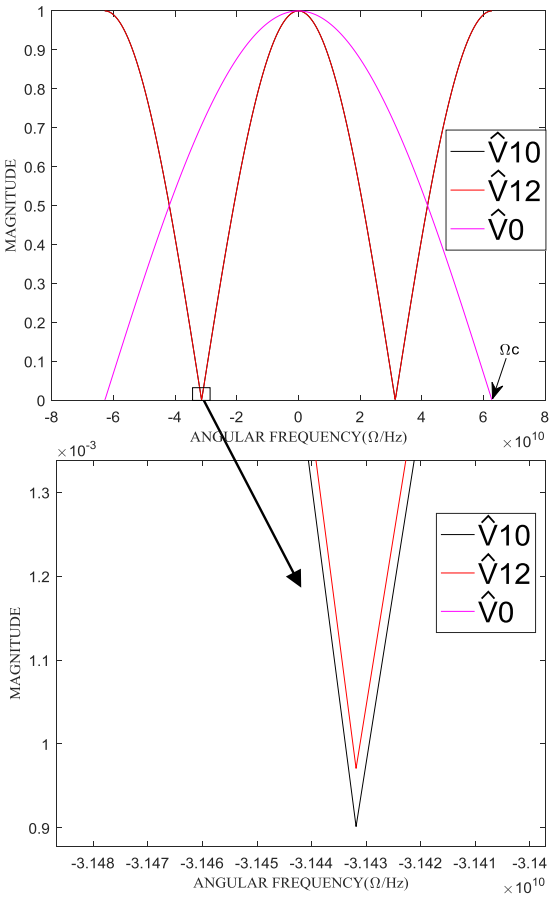

FIGURE 7. The amplitude-frequency curve of practical analog filters.

VI. SIMULATION RESULTS

To demonstrate the effectiveness of proposed HFB structure shown in Fig. 5 and calibration algorithm, a four-channel 20GS/s 12-bit FIADC system has been designed.

Reasonably assume that the analog filter transfer functions satisfy,

$$\begin{cases} \left|V_0\left(j\frac{\pi}{2T_S}\right)\right|^2 = \frac{1}{2} \\ \left|V_0\left(j\frac{\pi}{T_S}\right)\right|^2 = 0 \end{cases} \tag{36}$$

and

$$\begin{cases} \left|V_1\left(j\frac{\pi}{2T_S}\right)\right|^2 = 0 \\ \left|V_1\left(j\frac{\pi}{T_S}\right)\right|^2 = 1. \end{cases} \tag{37}$$

Based on the Genetic algorithm, we get transfer functions of the analog-filters, as shown in (38) and (39), as shown at the bottom of the next page. The amplitude-frequency curves of the third-order analog filters $V_0\left(j\frac{\omega}{T_s}\right)$ and $W_0\left(j\frac{\omega}{T_s}\right)$ are shown in Fig. 6(a) and amplitude-frequency curves of the fifth-order analog filters $V_1\left(j\frac{\omega}{T_s}\right)$ and $W_1\left(j\frac{\omega}{T_s}\right)$ are shown

TABLE 1. Actual errors and estimation errors.

type	Actual error	Estimation error	type	Actual error	Estimation error
ε_0	0.0012	0.0012	∂_0	0.0012	0.0013
ε_1	0.0010	0.0011	∂_1	0.0012	0.0012
ε_2	0.0013	0.0013	∂_2	0.0014	0.0013
ε_3	0.0014	0.0014	∂_3	0.0013	0.0013
ε_4	0.0012	0.0012	∂_4	0.0014	0.0014
ε_5	0.0015	0.0015	Δg_0	0.0025	0.0025
ε_6	0.0013	0.0014	Δg_1	0.023	0.023
ε_7	0.0013	0.0013	Δg_2	0.026	0.026
o_0	0.0100	0.0100	o_1	0.0012	0.0012
o_2	0.0210	0.0210	o_3	0.0019	0.0019

in Fig. 6(b). Then we assumed parameter errors according to practical experience, as Table 1 shown. The amplitude-frequency curves of practical analog filters which have deviations of ideal analog filters are shown in Fig. 7. Next, the proposed method in Section V is used to estimate the errors and corresponding digital synthesis filters are designed to calibrate the errors. The estimation results are shown in Table 1. Obviously, the proposed method is effective for estimating errors.

Respectively, define the distortion error function and aliasing error as

$$\begin{aligned} Dis &= \left|T_0\left(e^{j\omega}\right)\right| \\ Ali &= \sum_{P=1}^{3}\left|T_p\left(e^{j\omega}\right)\right|. \end{aligned} \tag{40}$$

Distortion error and aliasing error of system before calibration are shown in Fig. 8(a) and Fig. 8(b) respectively, and curves after calibration are shown in Fig. 9(a) and Fig. 9(b) respectively. After comparing Fig 8 and Fig 9, it can be seen that the aliasing error and the distortion error are reduced obviously, proving that the calibration is useful.

We can find that there are still some errors in Fig. 9. The errors have two sources. One is the estimation deviation of parameter in the analog filters. The other one lies in the digital synthesis filters. We design FIR digital filters based on the window function, which caused signal truncation, and accordingly lead to the error.

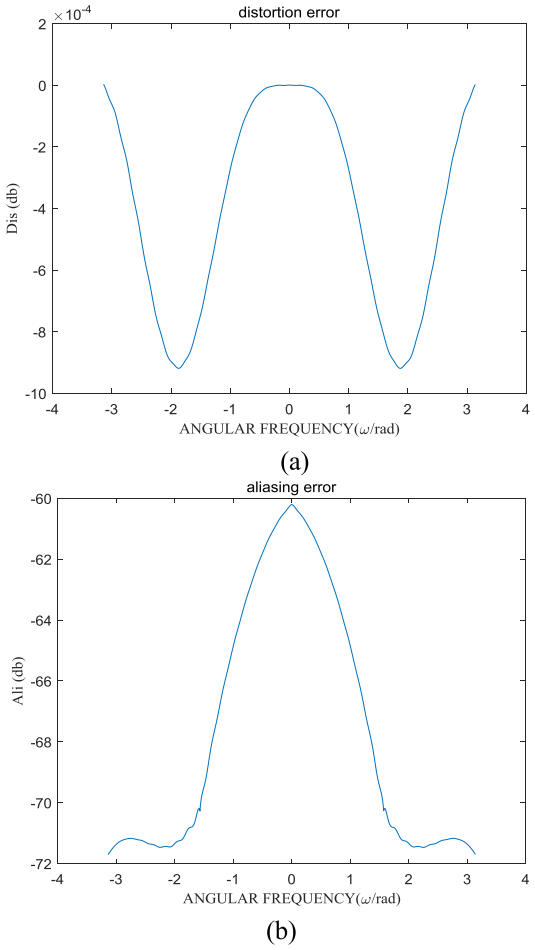

FIGURE 8. (a) Distortion error before calibration. (b) Aliasing error before calibration.

Define the average distortion error and average aliasing error can be obtained,

$$\begin{aligned} D_{avg} &= \int_{-\pi}^{\pi}\left|T_0\left(e^{j\omega}\right)\right|d\omega \\ A_{avg} &= \int_{-\pi}^{\pi}\sum_{P=1}^{3}\left|T_p\left(e^{j\omega}\right)\right|d\omega, \end{aligned} \tag{41}$$

thus the maximum distortion error and maximum aliasing error are

$$\begin{aligned} D_{\max} &= \max_{0<\omega<\pi}\left|T_0\left(e^{j\omega}\right)\right| \\ A_{\max} &= \max_{0<\omega<\pi}\left|T_p\left(e^{j\omega}\right)\right|. \end{aligned} \tag{42}$$

$$V_0\left(j\frac{\omega}{T_s}\right) = \frac{101.5355 + 10.2877\,(j\omega)^2}{101.5355 + 50.9470\,(j\omega) + 10.2877\,(j\omega)^2 + (j\omega)^3} \tag{38}$$

$$V_1\left(j\frac{\omega}{T_s}\right) = \frac{-14.0687\,(j\omega)^4 - 375.0379\,(j\omega)^2 - 839.7180}{(j\omega)^5 - 14.0687\,(j\omega)^4 + 94.9372\,(j\omega)^3 - 375.0379\,(j\omega)^2 + 839.5839\,(j\omega) - 839.718}. \tag{39}$$

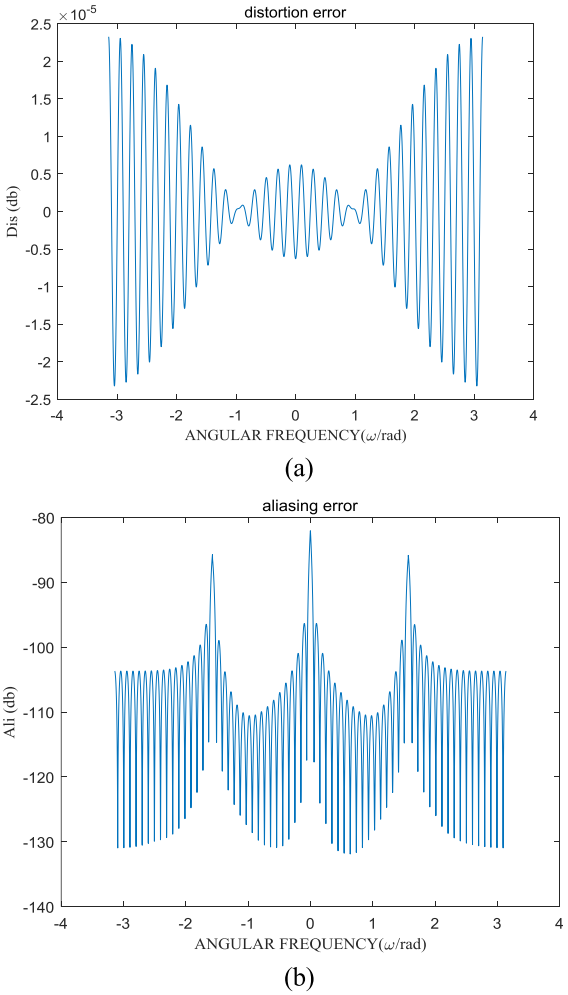

FIGURE 9. (a) Distortion error after calibration. (b) Aliasing error after calibration.

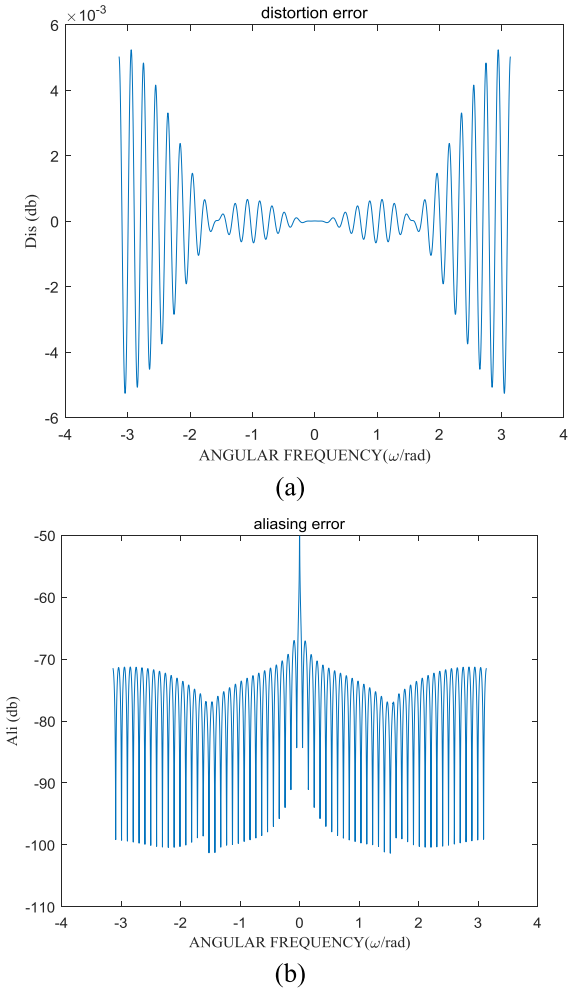

FIGURE 10. (a) Distortion error of traditional structure HFB. (b) Aliasing error of traditional structure HFB.

To make the system meet the requirement of 12-bit, the maximum distortion error should satisfy

$$|D_{\max} - 1| < 2^{-13}. \tag{43}$$

After calculation, the average distortion error is -6.8192×10^{-10} dB, and the average aliasing error is -104.8 dB. The maximum distortion error is smaller than 2.5×10^{-5} dB. It is obvious that the distortion error meets the design conditions in (43).

TIADC and FIADC have been detailedly compared in [8], and the conclusions indicate that the FIADC has a better mismatch suppression. Therefore, we do not compare them in this paper. Literature [22] has proposed a mismatch compensation algorithm based on the traditional HFB structure. We design a four-channel 20GS/s 12-bit FIADC system taking the method provided in the [22] as a reference. The HFB of this system consists of a third-order low-pass and three fifth-order band-pass Butterworth filters. Here we set the same errors as in the table 1. The distortion error and the aliasing error after calibrated by the calibration algorithm in the [22] are shown in Fig. (10).

It is obvious that the design scheme we proposed is superior to that proposed in [22]. Furthermore, the improved tree-structure of HFB only need three analog filters, whereas the traditional structure need four. Therefore, the analog circuit is simplified.

There are also many improved design methods based on traditional structures [17], [18], [11], which, However, are without considering the channel mismatch and analog filter deviation. Therefore, ignoring the effects of channel mismatch and analog filter deviation, we have designed two four-channel, 20GS/s HFB systems based on [17] and [18] respectively, as Table 2 shows. The order of the analog filters and the length of digital filters are the same.

We can see the improved tree-structure has smaller maximum distortion and aliasing error which affect resolution of HFB system. The reason is that the analog filters of the traditional structure should divide the entire input band perfectly without overlapping, but the analog analysis filters are not ideal low-pass and band-pass filters in practical design. the stopband and transition band of the analog filters and digital filters are unavoidable. There is no need for the

TABLE 2. Performance OF HFB for four-channel, 20GS/s case.

	Order of analog filters	Length of digital filters	Maximum distortion error	Maximum aliasing error
Structure in the paper	One third-order and two fifth-order	64	-5.7088×10^{-6} dB	-105.2104 dB
Structure in [17]	Four fifth-order	64	-0.0032 dB	-70.3021dB
Structure in [18]	Four fifth-order	64	-0.0007dB	-91.6253 dB

power complementarity-based structure to divide the frequency band. The transfer functions of analog analysis filters in this structure are symmetric in the real and imaginary axes, which can be implemented using sample passive RLC-circuit.

VII. CONCLUSION

This paper introduces an improved structure of HFB which only needs $M-1$ analog filters in M-channel HFB system. The proposed structure is a lot simpler than the traditional structure. Accordingly, an effective estimation and calibration technique of mismatch error is proposed, which exhibits an excellent effect based on simulation results. Further researches will realize this system in practical circuit.

REFERENCES

[1] X. Yi *et al.*, "Synchronous acquisition of multi-channel signals by single-channel ADC based on square wave modulation," *Rev. Sci. Instrum.*, vol. 88, no. 8, p. 085108, 2017.

[2] P. Monsurrò, F. Rosato, and A. Trifiletti, "New models for the calibration of four-channel time-interleaved ADCs using filter banks," *IEEE Trans. Circuits Syst. II, Exp. Briefs*, vol. 65, no. 2, pp. 141–145, Feb. 2017.

[3] C. Lelandais-Perrault, T. Petrescu, D. Poulton, P. Duhamel, and J. Oksman, "Wideband, bandpass, and versatile hybrid filter bank A/D conversion for software radio," *IEEE Trans. Circuits Syst. I, Reg. Papers*, vol. 56, no. 8, pp. 1772–1782, Aug. 2009.

[4] D. G. Nairn, "Time-interleaved analog-to-digital converters," in *Proc. IEEE CICC*, San Jose, CA, USA, Sep. 2008, pp. 289–296.

[5] J. Elbornsson and J. E. Eklund, "Blind estimation of timing errors in interleaved AD converters," in *Proc. IEEE ICASSP*, Salt Lake, UT, USA, May 2001, pp. 3913–3916.

[6] S. Huang and B. C. Levy, "Blind calibration of timing offsets for four-channel time-interleaved ADCs," *IEEE Trans. Circuits Syst. I, Reg. Papers*, vol. 54, no. 4, pp. 863–876, Apr. 2007.

[7] S. M. Jamal, D. Fu, N. C.-J. Chang, P. J. Hurst, and S. H. Lewis, "A 10-b 120-Msample/s time-interleaved analog-to-digital converter with digital background calibration," in *IEEE Int. Solid-State Circuits Conf. (ISSCC) Dig. Tech. Papers*, San Francisco, CA, USA, Feb. 2002, pp. 172–457.

[8] Q. Lei, Y. Zheng, and L. Siek, "Analysis and design of high performance frequency-interleaved ADC," in *Proc. IEEE ISCAS*, Beijing, China, May 2013, pp. 2022–2025.

[9] A. Petraglia and S. K. Mitra, "High-speed A/D conversion incorporating a QMF bank," *IEEE Trans. Instrum. Meas.*, vol. 41, no. 3, pp. 427–431, Jun. 1992.

[10] S. R. Velazquez, T. Q. Nguyen, S. R. Broadstone, and J. K. Roberge, "A hybrid filter bank approach to analog-to-digital conversion," in *Proc. IEEE-SP TFSA*, Philadelphia, PA, USA, Oct. 1994, pp. 116–119.

[11] S. R. Velazquez, T. Q. Nguyen, and S. R. Broadstone, "Design of hybrid filter banks for analog/digital conversion," *IEEE Trans. Signal Process.*, vol. 46, no. 4, pp. 956–967, Apr. 1998.

[12] L. Qiu, Y. Zheng, and L. Siek, "A filter bank mismatch calibration technique for frequency-interleaved ADCs," *Circuits, Syst., Signal Process.*, vol. 35, no. 11, pp. 3847–3862, Nov. 2016.

[13] L. Guo, S. Tian, Z. Wang, K. Yang, and L. Qiu, "Analysis of channel mismatch errors in frequency-interleaved ADC system," *Circuits, Syst., Signal Process.*, vol. 33, no. 12, pp. 3697–3712, Dec. 2014.

[14] D. E. Marelli, K. Mahata, and M. Fu, "Hybrid filterbank ADCs with blind filterbank estimation," *IEEE Trans. Circuits Syst. I, Reg. Papers*, vol. 58, no. 10, pp. 2446–2457, Mar. 2011.

[15] P. Lowenborg, H. Johansson, and L. Wanhammar, "A class of two-channel approximately perfect reconstruction hybrid analog/digital filter banks," in *Proc. IEEE ISCAS*, Geneva, Switzerland, May 2000, pp. 579–582.

[16] M. A. A. Pinheiro, P. B. Batalheiro, A. Petraglia, and M. R. Petraglia, "Improving the near-perfect hybrid filter bank performance in the presence of realization errors," in *Proc. IEEE ICASSP*, Washington, DC, USA, May 2001, pp. 1069–1072.

[17] W. Wang and Z.-J. Zhang, "Design of digital synthesis filters for hybrid filter bank A/D converters using semidefinite programming," *J. Netw.*, vol. 9, no. 5, pp. 99–104, May 2014.

[18] C. Yuan, W. Wang, and Z.-J. Zhang, "A modulated hybrid filter bank for wide-band analog-to-digital converters," *J. Multimedia*, vol. 9, no. 4, pp. 569–575, Apr. 2014.

[19] Z. Liu and M. Lin, "A frequency-translating hybrid architecture for wide-band analog-to-digital converters," in *Proc. IEEE ICSP*, Beijing, China, Aug. 2004, pp. 407–410.

[20] S. J. Mazlouman and S. Mirabbasi, "A frequency-translating hybrid architecture for wide-band analog-to-digital converters," *IEEE Trans. Circuits Syst. II, Exp. Briefs*, vol. 54, no. 7, pp. 576–580, Jul. 2007.

[21] D. E. Goldberg *et al.*, "Genetic algorithm in search optimization and machine learning," *Mach. Learn.*, vol. 3, no. 7, pp. 2104–2116, 1989.

[22] L. Qiu, Y. J. Zheng, and L. Siek, "Design of frequency-interleaved ADC with mismatch compensation," *Electron. Lett.*, vol. 50, no. 9, pp. 659–661, May 2014.

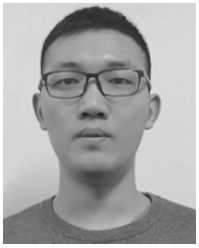

XIANGYU PENG was born in Henan, China, in 1994. He received the B.S. degree from the National University of Defense Technology, China, in 2016, where he is currently pursuing the master's degree. His current research interests include radar signal acquisition and processing.

JINGYU LI was born in Henan, China, in 1990. He received the B.S. degree from the Beijing Normal University in 2013 and the M.S. degree in communication engineering from the National University of Defense Technology, China, in 2015, where he is currently pursuing the Ph.D. degree. His current research interests include radar signal acquisition and processing.

XIAOTIAN ZHOU was born in Shandong, China, in 1994. He received the B.S. degree from the National University of Defense Technology, China, in 2016. He is currently with the Target Support Brigade of STCJOCC. His current research interests include the design of electronic circuits.

QIANQIANG LIN was born in Fujian, China, in 1983. He received the Ph.D. degree in electronic science and technology from the National University of Defense Technology, China, in 2013. His current research interests include radar signal acquisition, radar signal processing, and ISAR imaging.

ZENGPING CHEN received the B.S. and Ph.D. degrees from the National University of Defense Technology, Changsha, China, in 1987 and 1994, respectively. He is currently a Professor and a Ph.D. Supervisor with the National University of Defense Technology. His current research interests include signal processing, radar system, and automatic target recognition.